A TIR-SAVED effector mediates antiviral immunity via a conserved host signal

Deepak Kumar Choudhary, Dana Vassover, Himani Singla, Hadar Shukrun, and Uri Gophna

The Shmunis School of Biomedicine and Cancer Research, George S. Wise Faculty of Life Sciences, Tel Aviv University, Tel Aviv, Israel

Correspondence to: urigo@tauex.tau.ac.il

Abstract

Cyclic oligonucleotide-based anti-phage signalling systems (CBASS) are widespread prokaryotic antiviral defense mechanisms that function through coordinated cyclase-effector interactions. Upon sensing viral infection, the cyclase produces a signal molecule that activates effector function and causes cell dormancy or death. However, the evolutionary origins and functional independence of CBASS components remain unclear. Type II CBASS systems commonly employ TIR-SAVED domain effector proteins that deplete cellular NAD^+ during viral infection. Here, we demonstrate that a TIR-SAVED effector protein can operate as a standalone antiviral defense, causing significant growth inhibition and approximately 50% viral clearance during infection in the complete absence of its cognate cyclase. Remarkably, we show that the TIR-SAVED effector can sense cyclic di-AMP, a conserved second messenger produced by the host diadenylate cyclase DacZ, when the canonical CBASS signal is absent. This antiviral activity was associated with depletion of cellular NAD^+ and required intact conserved functional residues within both the TIR and SAVED domains. These findings reveal a novel mechanism of antiviral signalling that expands the functional repertoire of CBASS. They also provide insights into the modular evolution of complex prokaryotic immune systems, suggesting that what are now CBASS effectors might have evolved as independent defense components before being integrated into multi-protein systems.

Introduction

Bacterial and archaeal cells employ diverse antiviral defense mechanisms to combat viral infections. Cyclic-oligonucleotide-based anti-phage signalling systems (CBASS) are of particular interest, since they are common in prokaryotes, and are the ancestors of the animal innate immune factors OAS and C-GAS Sting[1]. These systems are found in almost 14% of bacteria[2,3] and can activate various cellular responses upon viral infection, triggering cell death or dormancy before the viruses can spread to sister cells [2,4–8]. To date, four types of CBASS systems have been identified in bacterial and archaeal populations, with approximately 39% being type II CBASS systems[2]. Typically, each type II CBASS gene cluster is composed of

genes encoding a cyclase, one or more effectors, and the ancillary proteins Cap2 and Cap3: a ubiquitin-like protein ligase and a deconjugating enzyme, respectively [2,7,9,10].

Many Bacterial type II CBASS Systems defend against viral infections through a TIR-SAVED domain effector protein that depletes cellular NAD^+ levels. Upon viral infection, a cyclic oligonucleotide is generated by the cyclase and sensed by the SAVED domain of the effector protein, which then enables the TIR domain-based NADase activity by oligomerization, which ultimately leads to cell dormancy or death[7,10]. This coordinated mechanism has been extensively characterized in bacterial systems, where mutation of the cyclase active site completely abolishes CBASS activity, reinforcing the view that the proteins of these systems function as interdependent components[10,11].

However, most if not all complex biological systems have evolved from pre-existing parts via a process that is often referred to as evolutionary tinkering[12,13]. The evolutionary origins and potential functional independence of CBASS components remain unknown. TIR domain proteins are ancient and widely distributed across prokaryotic antiviral systems [2,7,14–20], existing both as standalone defense proteins and as components of complex multi-protein systems[14]. Similarly, SAVED domains are found across diverse immunity contexts, including various CBASS types and type III CRISPR systems, suggesting potential functional versatility beyond their canonical signalling roles[2,7,21–25]. This raises the question if the fusion of these domains into one protein preceded their association with the cyclase, and whether CBASS effectors can function independently of their cognate cyclases or recognize alternative signalling molecules beyond their predicted substrates.

If effectors can operate autonomously, this would suggest that complex CBASS systems may have evolved through the recruitment and integration of pre-existing defense components, rather than co-evolution as obligate modules. Furthermore, the ability of effectors to recognize alternative signalling molecules could provide additional layers of antiviral protection and explain the remarkable diversity and widespread distribution of CBASS systems across bacterial and archaeal genomes[2].

Our previous work demonstrated that an archaeal Type II CBASS system in *Haloferax volcanii* (H-CBASS2) responds to chronic viral infection by inducing growth inhibition rather than triggering cell death[10], suggesting an alternative mechanism of action in halophilic archaea compared to the typical abortive infection responses observed in bacteria. Here, we investigate the functional independence of TIR-SAVED effector proteins from H-CBASS2. Using the chronically-infecting virus HFPV-1 and the model archaeon *H. volcanii*, we demonstrate that the H-TIR-SAVED effector can function as a standalone antiviral defense

system, causing growth inhibition and viral clearance in the complete absence of its cognate cyclase. Remarkably, we show that this independent activity depends on the recognition of cyclic di-AMP, a conserved signal secondary messenger produced by the host diadenylate cyclase DacZ, in the absence of the canonical cyclic trinucleotide signal typically associated with type II CBASS systems that are related in sequence and structure to HCBASS2. Our findings reveal a novel mechanism of antiviral signalling that expands the functional repertoire of known CBASS signals and provides insights into the evolution of complex prokaryotic immune systems.

Results

Expression of TIR–SAVED proteins lead to growth inhibition during viral infection, even in the absence of a H-CBASS2 cyclase

We recently showed that the type II CBASS system of *Haloferax* strain Atlit 48N (H-CBASS2) senses chronic virus infection and causes growth inhibition when expressed in *H. volcanii*[10]. This type II CBASS has a TIR-SAVED effector protein, which deplete NAD^+ following viral infection in the presence of a cyclic nucleotide signal[7,10].

To investigate the dependence of H-CBASS2 on the signal produced by its cognate cyclase we first cloned H-TIR-SAVED protein (Fig. 1A) separately into the high-copy replicating plasmid pTA927, which contains an inducible promoter, and transformed the constructs into *H. volcanii*, which does not have any CBASS system. We then infected the cells with the HFPV-1, a chronically-infecting virus[26], and selected virus-infected colonies expressing each individual protein to assess their physiological effects. Interestingly, we observed that virus-infected cells expressing H-TIR-SAVED, despite lacking both the E1-E2-JAB and cyclase proteins, exhibited substantial growth inhibition compared to non-infected cells or those carrying an empty vector (Fig. 1B). A slight growth inhibition was also observed upon H-TIR-SAVED expression, in the absence of virus infection, in *H. volcanii* compared to the control strain (Fig. 1B). We used qPCR to measure viral DNA levels in the supernatant and found that cells expressing H-TIR-SAVED showed a 20-30% reduction in viral DNA compared to control cells (Fig. 1C)

Next, we performed live-dead staining assays on logarithmic cultures of HFPV-1-infected cells expressing H-TIR-SAVED proteins. In agreement with our previous findings on the full CBASS system[10], no dead cells were observed in these cultures (Extended Fig. 1a). As expected, H-TIR-SAVED expression also did not affect the plaquing efficiency of HFPV-1(Fig. 1D). Similar to the full-length type II CBASS system[10], the expression of H-TIR-SAVED caused a growth delay but did not induce cell death, reinforcing the idea that type II CBASS systems and their

components do not function as a typical abortive infection mechanism, at least not during chronic HFPV-1 infection. We then investigated the long-term effects of viral infection by exposing cells expressing H-TIR-SAVED to room temperature conditions for 3-4 weeks. The virus-infected colonies of cells expressing the H-TIR-SAVED (NAD-depleting) effector exhibited noticeable bleaching compared to infected H-TIR-SAVED-negative control cells (Fig. 1E), similar to the results obtained previously with the full system[10]. As expected, subsequent live-dead assays after long-term virus exposure revealed a higher proportion of dead cells in virus-infected H-TIR-SAVED culture compared to infected controls (Extended Fig. 1b). We also observed that HFPV-1 infection caused more severe growth delay in cells expressing H-TIR-SAVED compared to those expressing full-length H-CBASS2[10] (Extended Fig. 2a). Additionally, virus-infected H-TIR-SAVED cells bleached more rapidly than cells expressing full-length H-CBASS2 (Extended Fig. 2b). Taken together, these results confirm that the TIR-SAVED effector is responsible for the bleaching activity previously observed for H-CBASS2, which probably results from depriving cells of NADPH required for the synthesis of isoprenoids, including carotenoids[27–29].

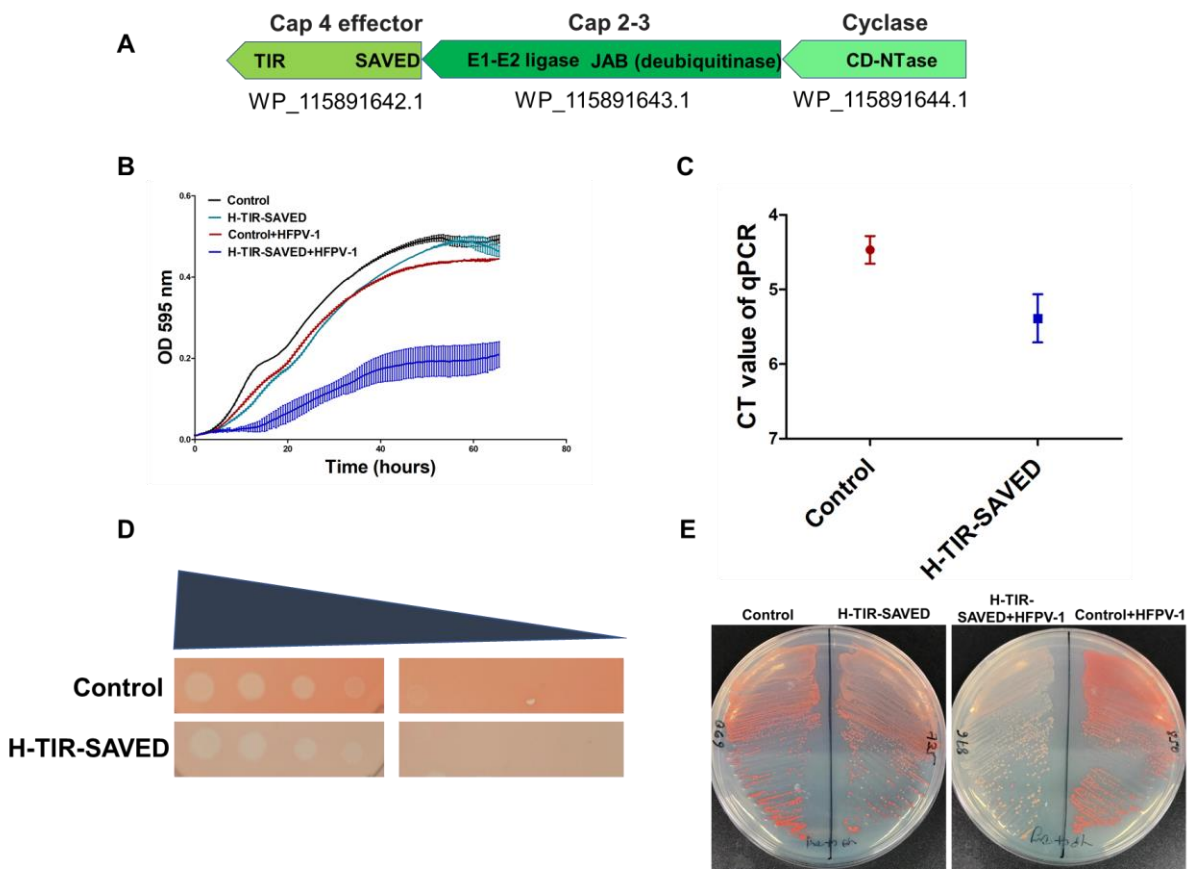

Figure 1. HFPV-1 infection causes growth delay in TIR–SAVED expressing in the absence of the CBASS cyclase. A) The H-CBASS2 operon. The H-CBASS2 TIR-SAVED effector (H-TIR-SAVED) gene was cloned into the pTA927 plasmid, regulated by an inducible tryptophanase promoter, and transformed into *H. volcanii* WR540.

HFPV-1 particles were then introduced into the H-TIR-SAVED expressing *H. volcanii* cells, and virus-infected colonies were selected through PCR screening. B) Growth curves of *H. volcanii* cells expressing H-TIR-SAVED under the tryptophan-inducible promoter (cyan) and control cells (empty vector, black), in the absence of viral infection, virus-infected H-TIR-SAVED-expressing cells (blue) under the tryptophan-inducible promoter and infected control cells, with an empty pTA927 (red). Values represent the mean ± SE of at least 3 biologicals replicates, each with three technical replicates. C) Viral DNA concentration in the supernatant of HFPV-1 infected *H. volcanii* cells after 72 hours of growth represented as Ct values determined using primers specific to the HFPV-1 genome (mean ± SE of three biological replicates). D) Plating efficiency of HFPV-1 measured by a plaque assay conducted using 10-fold serial dilutions of virus stock (the left-most dilution is a 10^{-4} virus suspension). H-TIR-SAVED expressing cells, as well as control cells with an empty vector, were mixed with 0.02% top agar and plated onto rich medium. Then, 3 µL of serial dilutions of HFPV-1 were spotted onto the plates to measure plaquing efficiency. The images shown are representative of at least three biological replicates. E) Bleaching of virus-infected H-TIR-SAVED-expressing *H. volcanii* colonies. Representative images of colony color for *H. volcanii* cells infected with HFPV-1 using *H. volcanii* strains expressing H-TIR-SAVED, either with or without viral infection, along with a control containing an empty vector. A 20 µL log-phase culture was streaked onto fresh plates, which were incubated at 45°C for 4-5 days. After growth became visible, the plates were stored at room temperature for 3-4 weeks, and images were captured.

The TIR-SAVED effector protein depletes NAD^+ in virus-infected cells, In the absence of the CBASS cyclase

Previous studies have demonstrated that type II CBASS systems detect viral infection through their cyclase proteins, which then produce cyclic signalling molecules that are sensed by effectors, ultimately triggering cell death or dormancy[7].Accordingly, our previous results showed that inactivating the cyclase by mutation abolished the H-CBASS2 activity during viral infection[10]. This raised the question of whether the observed growth delay in H-TIR-SAVED-expressing cells was caused by NAD^+ depletion. To determine whether the H-TIR-SAVED protein was able to deplete cellular NAD^+ levels in the absence of a cyclase we measured total NAD levels in logarithmic-phase cultures of HFPV-1-infected cells expressing H-TIR-SAVED. Interestingly, we found that total NAD levels decreased in virus-infected H-TIR-SAVED-expressing cells compared to infected controls containing an empty vector (Fig. 2A). In contrast, total NAD levels in infected cells expressing the full H-CBASS2 remained unchanged during logarithmic growth[10]. Moreover, we also observed a substantial reduction in total NAD levels, in infected bleached colonies expressing H-TIR-SAVED in the absence of a virus (Fig. 2B). Notably, when measuring NAD^+ levels, we observed that infected H-TIR-SAVED-expressing cells showed a two-fold greater decrease compared to cells expressing the full-length H-CBASS2 (Extended Fig. 2c). Next, we generated the H-TIR-SAVED and *Microbacterium ketosireducens* TIR-SAVED structures using AlphaFold 3[30]. We then compared the H-TIR-SAVED structure with the *M. ketosireducens* TIR-SAVED structure using Chimera and created a homology model [31], which revealed a high degree of structural similarity (RMSD between 196 pruned atom pairs is 1.188 angstroms; (across all 383 pairs:

3.757) (Fig. 2C). Further analysis identified E80 as the active-site residue in the TIR domain, which we mutated to glutamine (E80Q). Notably, previous studies reported that this mutation in *M. ketosireducens* TIR-SAVED abolished both NAD depletion and phage defense[7,32]. Consistent with these findings, the E80Q mutation in H-TIR-SAVED fully restored NAD levels and partially rescued the growth phenotype (Fig. 2D&E) in H-TIR-SAVED -expressing infected cells. Furthermore, we did not observe bleached colonies in virus-infected cells after introducing this mutation (Extended Fig. 3).

Recent studies have shown that TIR-SAVED oligomerizes and becomes active in the presence of cA3 signalling molecules. This multimerization is crucial for its function, as mutations in the SAVED domain active site disrupt signal binding (specifically to cA3)[7], rendering the protein monomeric and inactive. We investigated whether structurally analogous amino acids in H-TIR-SAVED would abolish its activity, which would indicate that, like a typical CBASS system, the H-SAVED domain binds specific signalling molecules in response to infection. To test this hypothesis, we introduced R195E and F388A mutations separately into the H-TIR-SAVED active site and found that the F388A mutation partially reversed the growth delay, partially restored NAD levels, and prevented the colony bleaching caused by HFPV-1 infection (Fig. 2F, Extended Fig. 4). This result indicates that, like a typical CBASS system, the SAVED domain must bind a specific signalling molecule in order to be active during infection.

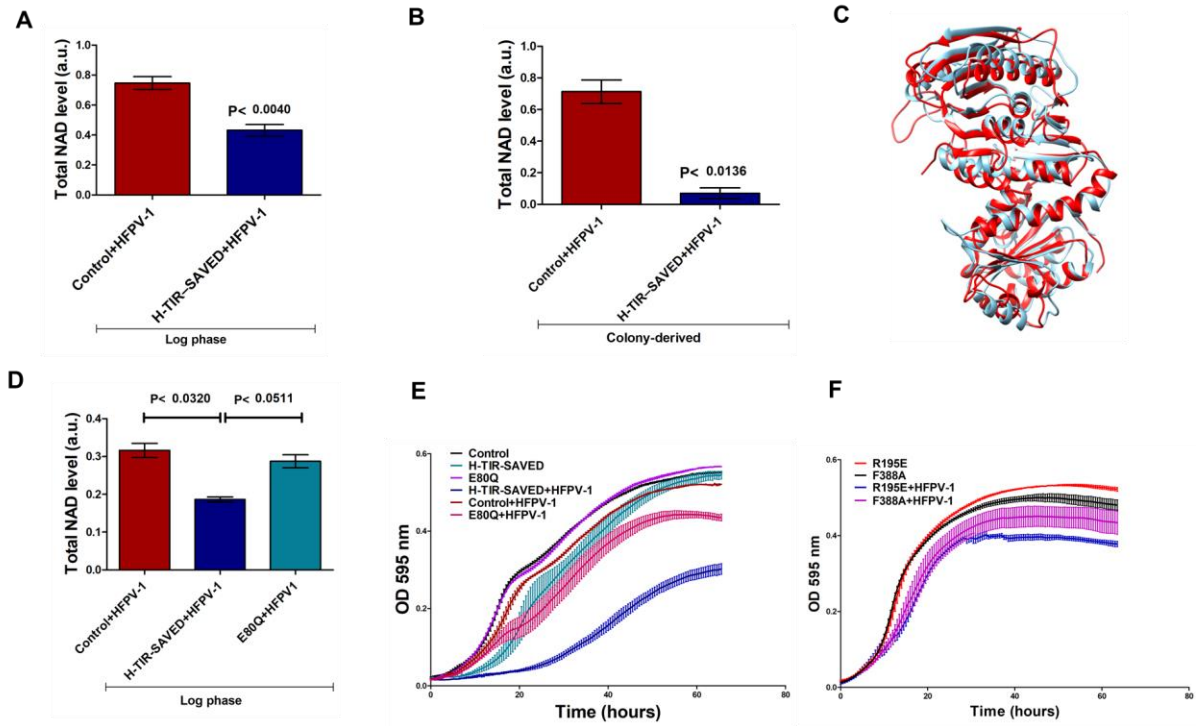

Figure 2. TIR-SAVED protein reduces NAD^+ levels in virus-infected cells independently of CBASS cyclase activity. A) NAD^+ levels in *H. volcanii* strains expressing H-TIR-SAVED following virus infection. Log-phase cultures with equal cell numbers were collected, and total NAD^+ levels were measured using the NAD/NADH Quantification Kit. B) NAD^+ levels in cells from bleached colonies. Bleached cells incubated for 3–4 weeks were resuspended in fresh medium, and equal protein-normalised biomass from each strain was used to quantify total NAD^+. A and B: Data represent results from three independent experiments. NAD^+ values of the different strains were compared using a paired sample t-test. C) 3D structural alignment comparing predicted H-TIR-SAVED and *M. ketosireducens* TIR-SAVED structures. Both structures were generated using AlphaFold 3 and aligned using ChimeraX software (RMSD = 3.757 Å). D) NAD^+ levels in *H. volcanii* strains expressing the Q80E mutation in TIR-SAVED protein. Strains were grown to log phase and NAD^+ levels were measured following the protocol described. Data are representative of three independent experiments. Statistical analysis was performed using a paired t-test. E) Growth curves showing the effect of the E80Q mutation in the H-TIR-SAVED protein. E80Q without infection is shown in purple, and with infection in pink. Control strains are shown in black (uninfected) and red (infected). Wild-type H-TIR-SAVED is shown in cyan (uninfected) and blue (infected). E) Growth curves of H-TIR-SAVED mutants R195E and F388A with and without viral infection. R195E is shown in red (uninfected) and blue (infected), while F388A is shown in black (uninfected) and pink (infected). E and F: Values represent the mean ± SE of at least three biological replicates, each with three technical replicates.

H-TIR-SAVED proteins sense cyclic di-AMP, a signaling molecule produced by a conserved host enzyme

Since introducing mutations in the signal binding site of H-TIR-SAVED abolished activity, this implied that a signalling molecule is required, which must be generated by a host enzyme in the absence of a cyclase during viral infection. Since H-TIR-SAVED is induced and may adopt an open conformation, it could potentially bind to molecules resembling its predicted substrate cAAG that are somehow produced as a result of membrane stress triggered by viral infection. The obvious candidate in the case of *H. volcanii* is the essential secondary messenger molecule cyclic-di-AMP (c-di-AMP)[33,34]. This molecule is produced by the diadenylate cyclase DacZ and has been shown to be essential, required for osmoregulation and, strikingly, toxic when its concentration rises above a certain threshold within cells[33,34]. Some diadenylate cyclases are found in proximity to CBASS gene clusters, and have been suggested to sense phage infection by responding to membrane stress[35,36].To test this hypothesis, we used *H. volcanii* strains with reduced and constitutive DacZ expression, exhibiting approximately 50% reduction in activity relative to basal levels[33]. We then introduced the H-TIR-SAVED protein along with HFPV-1 virus into these low c-di-AMP cells. Notably, cells expressing H-TIR-SAVED in these strains showed substantially milder growth inhibition when infected with HFPV-1 (Fig. 3A). Furthermore, we added exogenous c-di-AMP to cells expressing either the full H-CBASS2 and H-TIR-SAVED proteins without viral infection and performed growth analyses. Interestingly, we found that in the presence of external c-di-AMP, the H-TIR-SAVED protein caused growth inhibition even in the absence of virus. We also observed a small effect on the

222 full-length CBASS system (Fig. 3B). Notably, we did not observe any effect of c-di-AMP when
223 we used strains with mutations in the TIR and SAVED domain proteins (Fig. 3C), as expected.

224 Next, we measured total NAD levels in cells expressing H-TIR-SAVED following
225 supplementation with exogenous c-di-AMP. Interestingly, total NAD levels were reduced in H-
226 TIR-SAVED-expressing cells compared to treated control cells containing an empty vector
227 (Fig. 3D), upon c-di-AMP supplementation. Taken together, these results indicate that the H-
228 CBASS TIR-SAVED effectors responds to c-di-AMP signalling, in the absence of its cognate
229 CBASS signal.

230

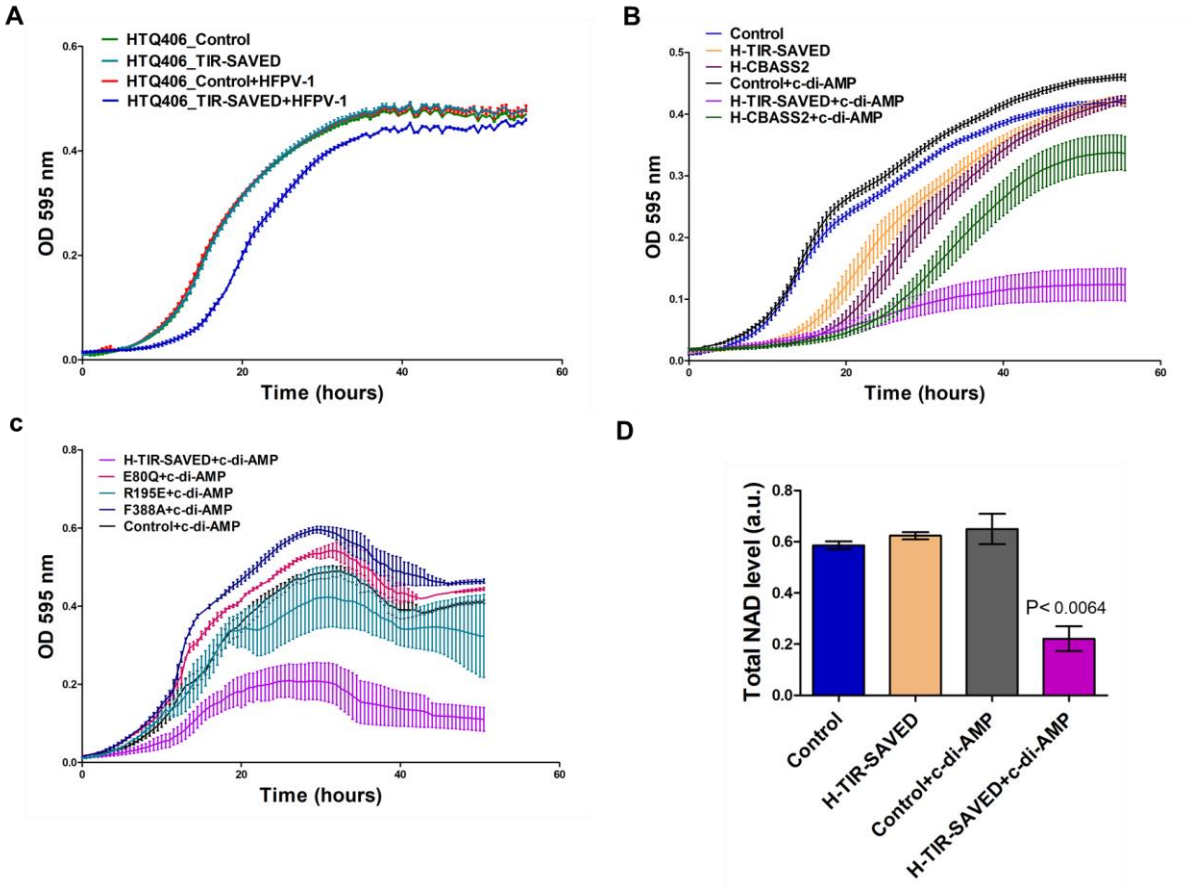

231

232 **Figure 3. H-TIR-SAVED senses the physiological stress molecule cyclic di-AMP**. A) Growth curves of cells of
233 *H. volcanii* strain HTQ406 that has reduced intracellular c-di-AMP levels[33]. H-TIR-SAVED was expressed in
234 HTQ406 cells that were infected with HFPV-1. Infected H-TIR-SAVED-expressing cells are shown in blue, infected
235 controls with empty vector in red, uninfected H-TIR-SAVED-expressing cells in cyan, and uninfected controls with
236 empty vector in green. B) Growth analysis of *H. volcanii* strains expressing H-CBASS2 (green) or H-TIR-SAVED
237 (purple) in the presence of exogenous c-di-AMP, compared to untreated H-CBASS2 or H-TIR-SAVED-expressing
238 cells (dark purple) or yellow, respectively). c-di-AMP-Treated and untreated control cells are shown in black and
239 blue. C) Growth curves of strains carrying mutations in the TIR and SAVED domains in the presence of c-di-AMP.
240 The wild-type H-TIR-SAVED strain with c-di-AMP is shown in purple, and its corresponding control in black. Mutants
241 E80Q (TIR domain), R195E, and F388A (SAVED domain) are shown in pink, cyan, and blue, respectively. Values

242 represent the mean ± SE of at least three biological replicates, each with three technical replicates. D) NAD^+ levels
243 in *H. volcanii* expressing H-TIR-SAVED following c-di-AMP treatment.
244 Log-phase cultures of c-di-AMP-treated and untreated cells, normalized to equal cell numbers by OD, were
245 collected, and total NAD^+ levels were measured as described in the Methods. D: Data represent results from at
246 least three independent experiments. NAD^+ values of the different strains were compared using a paired sample t-
247 test.
248

249 **HFPV-1 infection increases cyclic di-AMP levels in *H. volcanii* cells**

250 Having established that H-TIR-SAVED proteins sense c-di-AMP produced by DacZ upon virus
251 infection, we next tested whether virus infection can increase the production of cellular c-di-
252 AMP. We therefore measured c-di-AMP levels in log-phase *H. volcanii* cells with or without
253 HFPV-1 infection. Interestingly, we found that virus-infected cells had almost 25% higher c-di-
254 AMP levels compared to control cells (Fig. 4A). These results demonstrate that virus infection
255 directly stimulates c-di-AMP production in *H. volcanii*, thereby providing the necessary signal
256 for H-TIR-SAVED activation.

257 **H-TIR-SAVED clears a chronic virus infection in *H. volcanii* cells**

258 We have observed that expression of full-length CBASS2 (H-CBASS2) is able to clear chronic
259 virus infection after several passages in rich medium[10]. Additionally, expression of H-TIR-
260 SAVED shows a stronger growth inhibition than the H-CBASS2 system (Extended Fig. 2a).
261 Therefore, we next investigated whether H-TIR-SAVED eliminates the virus as effectively as
262 the complete H-CBASS2 system does. We therefore cultured HFPV-1-infected *H. volcanii*
263 cells in liquid medium until late log or stationary phase, comparing cultures either expressing
264 or not expressing H-TIR-SAVED. These cultures were then used to inoculate fresh medium,
265 and this process was repeated for 6 passages. Samples were collected at passages 3 for
266 analysis. We plated diluted cultures on solid media and screened 25-30 colonies from each
267 replicate by PCR to detect the presence of HFPV-1 DNA. Interestingly, virus-infected cells
268 expressing the H-TIR-SAVED protein demonstrated significant antiviral efficacy despite the
269 absence of both E1-E2-JAB and cyclase proteins. By passage 3, these cells showed
270 approximately 50% virus clearance (Fig. 4B). This antiviral effect became even more
271 pronounced by passage 6, where nearly all colonies from H-TIR-SAVED-expressing cultures
272 had undetectable levels of viral DNA across all three biological replicates. In contrast, almost
273 all control colonies that did not express H-TIR-SAVED maintained detectable viral DNA
274 presence (Fig. 4B). Taken together, the independent antiviral and NADase activities, and the
275 effect on growth strongly suggest that the H-TIR-SAVED protein can function as an
276 **independent** immune effector in *H. volcanii* and can respond to viral infection by sensing c-
277 di-AMP signals produced by different cyclase such as DacZ within the cell, rather than being
278 limited to detecting their putative cAAG signal (Fig. 4C).

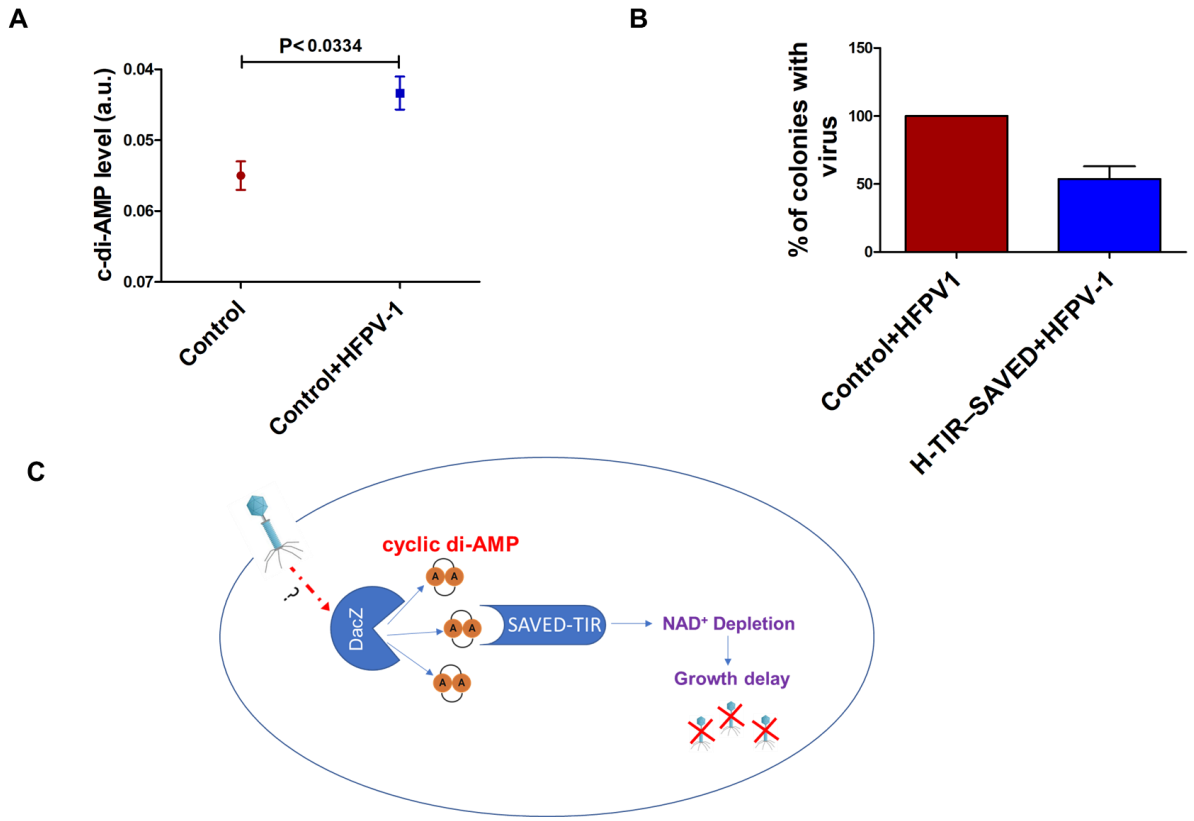

Figure 4. Expression of H-TIR-SAVED leads to clearance of chronic virus infection in *H. volcanii*. A) Elevated c-di-AMP Levels in *H. volcanii* following Viral Infection. Log-phase cultures with equal cell numbers were collected, and total c-di-AMP levels were measured using the c-di-AMP ELISA Kit. The absorbance at 450 nm, measured spectrophotometrically, reflects the amount of cyclic di-AMP-HRP tracer bound to the wells and is inversely proportional to the concentration of free c-di-AMP present during the incubation period. B) Ratio of virus-free colonies vs. virus-infected after three passages in rich medium containing tryptophan. *H. volcanii* strain infected with HFPV-1 and expressing H-TIR-SAVED was compared to a virus-infected control strain, and virus presence was determined using colony PCR. C) Proposed model for the mechanism of action of the TIR-SAVED effector in the absence of a cognate cyclase. Upon HFPV-1 infection, the DacZ protein senses membrane stress caused by the presence of the virus and produces c-di-AMP signalling molecules. The SAVED domain detects the c-di-AMP signal, triggering activation of the TIR domain. The activated TIR domain then depletes cellular NAD^+ levels, leading to growth delay and eventual bleaching and death.

Discussion

Here we show that the TIR-SAVED effector of a type II CBASS can act independently as an antiviral defense, and is capable of inducing growth inhibition during infection in the absence of cyclase protein (Fig. 1B). Such independent activity may provide a more robust defense system that is less sensitive to anti-defense mechanisms, such as anti-CBASS (Acb) proteins that sequester signal molecules and inhibit CBASS-based immunity[37,38]. This is consistent with a system that has evolved to have co-dependency between its components. Taken together, these results help explain how complex CBASS systems evolved from their individual

302 components, prior to becoming inter-dependent. TIR-domain proteins are found in many
303 different anti-phage systems, and there are even single protein TIR-domain systems[14], and
304 thus could have been recruited for defensive roles before becoming associated with a cognate
305 cyclase. Consistent with previous studies in other organisms, we show that the TIR-SAVED
306 effector can cause growth inhibition by depleting NAD^+ levels in infected cells[7,10]. Interestingly,
307 we found that the expression of TIR-SAVED without the other CBASS components also led to
308 a significant reduction in NAD^+ levels in virus-infected *H. volcanii* cells (Fig. 2A&B), confirming
309 this domain's critical role in the observed growth inhibition. The E80Q mutation in the catalytic
310 site of the TIR domain partially reversed the growth phenotype and fully prevented the NAD^+
311 depletion caused by virus infection in cells expressing the stand-alone TIR-SAVED protein
312 (Fig. 2D&E).

313 We further show that the SAVED domain's ability to mediate antiviral responses depends on
314 specific conserved residues required for signal sensing. The rescue of the growth phenotype
315 and suppression of bleaching by the F388A mutation (which is important for cA3-binding in b
316 bacteria[7] (Fig. 2F) support a role for the SAVED domain as a signal sensor, likely detecting a
317 cyclic nucleotide signal even in the absence of the canonical cyclase. This is further supported
318 by our observation that H-TIR–SAVED can sense cyclic di-AMP (c-di-AMP), representing a
319 novel twist in the study of CBASS signalling specificity. The substantial rescue of growth
320 inhibition in strains with reduced DacZ expression (Fig. 3A), along with the induction of growth
321 arrest by exogenous c-di-AMP in the absence of viral infection (Fig. 3B&C), provides strong
322 evidence that this effector protein has evolved to recognize endogenous signalling molecules
323 beyond the canonical cA3G produced by CBASS cyclases. These results suggest that while
324 the SAVED domain retains its ligand-binding role, it has broad enough specificity to recognize
325 structurally related cyclic nucleotides beyond its cognate trinucleotide, which is predicted by
326 structural similarity to be cAAG. This expanded signal-recognition capacity may explain the
327 widespread presence of SAVED domains across diverse antiviral immune systems, including
328 various CBASS types as well as type III CRISPR systems[2,5,7,39].

329 Our observation that viral infection can increase c-di-AMP levels in *H volcanii* is not really
330 surprising (Fig. 4A). C-di-AMP plays several key roles in bacterial physiology, including
331 responses to osmotic stress and protecting DNA integrity[40–42]. While membrane stress is more
332 typical to early stages of viral infection, at least in bacteria, DNA damage is generally not
333 considered to be phage associated. However, replication of phage genomes often includes
334 DNA open ends, which are indistinguishable from DNA breaks at the molecular level, and
335 could therefore indicate viral replication and trigger a defensive function. Notably, many genes
336 encoding DacZ enzymes naturally co-occur with CBASS systems[35,36], suggesting a potential
337 link between viral infection, c-di-AMP signalling, and CBASS activation. This also could explain

338 why prokaryotes typically encode a complete CBASS system rather than a standalone TIR-
339 SAVED effector. If TIR-SAVED operated independently based on c-di-AMP signalling alone, it
340 could respond to various physiological stresses in the absence of infection. Such response
341 would not be beneficial for the cells since a response that delays growth and eventually can
342 result in cell death should be reserved exclusively to stopping the spread of viral infection
343 rather triggered during general stress situations.

344 These findings of cyclase-independent effector function are in contrast to our previous
345 observations that when the whole H-CBASS2 cluster was expressed together, and cyclase
346 activity was abolished by point mutation[10,43],this resulted in complete abolishment of CBASS
347 activity. This indicates that either the E1-E2 protein, the H-CBASS2 cyclase or both can
348 modulate the effector function until the cyclase produces enough specific signal. The
349 molecular basis for this molecular remains to be elucidated, but one may speculate that the
350 complete system is better for cells than the lone TIR-SAVED effector because it is less likely
351 to respond to spurious membrane stress in a way which is harmful, in the absence of viral
352 infection.

353 Altogether, our findings suggest that H-TIR-SAVED proteins can function as standalone
354 immune effectors that sense c-di-AMP signals produced by different cellular cyclases to detect
355 viral infection and mediate defense responses. This expands the functional repertoire of
356 CBASS effectors beyond their originally defined signalling context and highlights a more
357 modular, signal-flexible architecture in immunity, which could extend beyond archaea to many
358 Gram-positive bacteria whose genomes encode both *dacZ* and CBASS.

359 **Methods**

360 **Culture conditions-** The Haloferax wild-type strains were regularly cultured at 45°C in either
361 Hv-YPC or Hv-Ca/Hv-Enhanced Ca medium. *Haloferax volcanii* transformants were selected
362 and grown in either Hv-Ca or Hv-Enhanced Ca (Hv-ECa) medium. Thymidine (40 µg/ml) and
363 tryptophan (50 µg/ml) were added when necessary. Bacterial strains were cultured at 37°C in
364 LB medium, or in LB medium supplemented with ampicillin for strains containing plasmids.

365 **Cloning and mutagenesis-** The *Haloferax* 48N TIR-SAVED proteins of the CBASS type II
366 system were cloned into the high-copy replicating plasmid pTA927 (which contains the
367 tryptophanase inducible promoter) using the Gibson assembly method. DNA fragments for the
368 inserts along with the plasmid vectors, were first PCR-amplified using specific primers and
369 either Phusion or KAPA-HiFi DNA polymerase. The PCR-amplified plasmids and DNA
370 fragments were purified using the Wizard® SV Gel and PCR Clean-Up Kit (Promega), followed
371 by DpnI digestion of the purified plasmids. The purified DNA fragments and plasmids were
372 then ligated using the Gibson assembly protocol (Gibson et al., 2009). The constructed

373 plasmids were introduced into *E. coli* DH12S cells through electroporation. The clones were
374 verified using PCR, and the plasmids were subsequently isolated using Sigma-Aldrich's
375 GenElute™ Plasmid Miniprep Kit. The purified plasmids were then introduced into *H. volcanii*
376 strains following previously published protocols (Halohandbook).

377 **Mutagenesis** - The TIR-dead variant of H-TIR-SAVED cloned into pTA927, was generated by
378 replacing the conserved glutamic acid at position 80 with glutamine using site-directed
379 mutagenesis. Similarly, mutations in the SAVED domain of H-TIR-SAVED, cloned into pTA927,
380 were introduced by substituting the conserved arginine at position 195 with glutamic acid, and
381 the phenylalanine at position 388 with alanine, using site-directed mutagenesis. All the
382 mutation was confirmed through sequencing.

383 **Transformation with HFPV-1-** *H. volcanii* cultures were grown overnight until reaching log
384 phase and collected by centrifugation (6,500 rpm, 5 min). The cell pellet was carefully
385 resuspended in 200 µl of spheroplasting solution (1 M NaCl, 27 mM KCl, 50 mM Tris-HCl, 15%
386 sucrose). The cells were treated with 0.5 M EDTA (pH 8) to remove divalent cations. After 10
387 minutes at room temperature, concentrated HFPV-1 particles (5-10 µl) were added and
388 incubated for 5 minutes. The suspension was then mixed gently with 250 µL of 60% PEG600
389 and incubated for 1 hour at room temperature. The cells were washed with 1 ml regeneration
390 solution (Hv-YPC+ media containing 15% sucrose) and resuspended in the same media. The
391 culture was first incubated statically at 28°C for 3 hours, followed by another 3-hour incubation
392 with shaking. The cells were then serially diluted, plated, and individual colonies were
393 screened for successful HFPV-1 infection using virus-specific PCR primers.

394 **Growth curves-** The strains were cultured overnight in Hv-ECa medium supplemented with
395 thymidine and tryptophan until reaching log phase. The cultures were then diluted in fresh Hv-
396 ECa medium containing thymidine and tryptophan to achieve an initial OD of 0.03-0.05. For
397 induction experiments, L-tryptophan was added to a final concentration of 2 mM. The diluted
398 cultures were grown in 96-well plates at 42°C with continuous shaking for 72 hours. Growth
399 was monitored by measuring optical density (OD595nm) at 30-minute intervals using a Biotek
400 ELX808IU-PC microplate reader. Each strain was tested in at least three biological replicates,
401 with each biological replicate consisting of three technical replicates.

402 **Growth curve with external cyclic di-AMP.** Growth experiments were performed using
403 uninfected cells expressing H-TIR-SAVED and a control strain containing the empty plasmid.
404 Each strain was grown overnight in Hv-ECa medium supplemented with thymidine and
405 tryptophan to log phase, then diluted to an OD_{600} of 0.03-0.05 in fresh medium containing 1
406 µM cyclic di-AMP. The cultures were incubated at 45°C with continuous shaking for 72 hours.
407 Growth was monitored by measuring optical density as described above.

408 **Growth curve with lower cyclic di-AMP -** To examine the effect of cyclic di-AMP, the H-TIR-
409 SAVED gene was first cloned into pTA927. Both this construct and the empty plasmid (control)
410 were transformed into *H. volcanii* strain HTQ406, which has approximately 50% lower
411 intracellular c-di-AMP levels[33]. The HTQ406 strain expressing H-TIR-SAVED was then
412 infected with HFPV-1 virus as described above. The cultures were incubated at 45°C with
413 continuous shaking for 72 hours. Growth was monitored by measuring optical density as
414 described above.

415 **Live/Dead staining-** Cell viability in virus-infected *H. volcanii* strains expressing H-TIR-
416 SAVED was assessed using the LIVE/DEAD bacterial Viability Kit (Thermo-Fisher, Ref-
417 L13152). Overnight cultures were diluted in fresh medium to an OD of 0.03-0.05 and grown at
418 45°C with shaking until reaching logarithmic phase. Aliquots of 100 µl from each culture were
419 transferred to 1 ml Eppendorf tubes. The cells were stained by adding 10 µl each of Propidium
420 iodide and SYTO9 dyes from their respective stock solutions. After incubating in darkness for
421 15-20 minutes to allow dye uptake, 10 µl of each stained culture was examined under a Leica
422 sp8 confocal microscope at 20x and 40x magnification. For analysing dead cells in bleached
423 colonies, cells were collected directly from plates containing bleached colonies and
424 suspended in 100 µl of Hv-ECa medium. The cell suspension was washed twice with Hv-ECa
425 medium before proceeding with the previously described microscopy staining and imaging
426 protocol.

427 **Plate colony pigmentation assays-** Strains were grown overnight until reaching log phase,
428 then diluted in fresh medium to OD 0.05. From each diluted culture, 20 µl was streaked onto
429 fresh plates and incubated at 45°C for 4-5 days. After initial growth, the plates were stored at
430 room temperature for 3-5 weeks, with images documented every three days.

431 **NADase assay-** Total cellular NAD was quantified using the NAD/NADH Quantification Kit
432 (Sigma-Aldrich, MAK037). Cultures were grown to late log phase, and equivalent cell numbers
433 (normalized by optical density) were collected and washed twice with cold Hv-Ca media. The
434 cells were pelleted by centrifugation (3000 rpm, 5 min) in 1.5 ml microcentrifuge tubes. Each
435 pellet was resuspended in 400 µl of NADH/NAD extraction buffer and lysed using two rounds
436 of sonication. The lysates were centrifuged (13,000 rpm, 10 min), and the supernatants were
437 filtered through Amicon 10 kDa cut-off spin filters to remove proteins. For the assay, 50 µl of
438 each deproteinized sample was transferred to a 96-well plate. A master reaction mixture (98
439 µl NAD cycling buffer + 2 µl NAD cycling enzyme mix) was prepared, and 100 µl was added
440 to each well. After 5 minutes of incubation at room temperature, 10 µl of NADH Developer was
441 added per well. The plates were incubated at room temperature for 1-2 hours, followed by
442 absorbance measurement at 450 nm. Bleached colonies were collected directly from plates

443 and suspended in 1 ml of cold Hv-Ca media, followed by two washing steps. The cells were
444 pelleted by centrifugation (3000 rpm, 5 min) in 1.5 ml microcentrifuge tubes. Each pellet was
445 resuspended in 400 µl of NADH/NAD extraction buffer and lysed using two rounds of
446 sonication. Protein concentration in the lysates was determined using the Bradford assay
447 before proceeding with the NAD quantification protocol as previously described.

448 **Cyclic di-AMP level quantification** - Total cellular c-di-AMP levels were quantified using the
449 c-di-AMP Quantification Kit (Cayman chemical, Cyclic di-AMP ELISA Kit Item No. 501960).
450 Cultures were grown to log phase, and equivalent cell numbers (normalized by optical density)
451 were collected and washed with cold Hv-Ca media. The cells were pelleted by centrifugation
452 (5,000 rpm, 5 min) in 1.5 ml microcentrifuge tubes. Each pellet was resuspended in 400 µl of
453 lysis buffer and lysed using two rounds of sonication. The lysates were centrifuged (13,000
454 rpm, 10 min), and the supernatants were filtered through Amicon 10 kDa cut-off spin filters to
455 remove proteins. A 96-well ELISA plate was washed five times with washing buffer. For the
456 assay, 50 µl of each sample was transferred to the wells. Subsequently, 50 µl of c-di-AMP
457 HRP tracer was added to each well except TA and blank wells, and 50 µl of c-di-AMP ELISA
458 monoclonal antibody was added to each well except blank, TA, and NSB wells. The plate was
459 incubated for two hours at room temperature with orbital shaking. After incubation, all wells
460 were emptied and washed five times with wash buffer. Then, 175 µl of TMB substrate solution
461 was added to each well and incubated for 30 minutes on an orbital shaker. Finally, 75 µl of
462 HRP stop solution was added to each well, and absorbance was measured at 450 nm. The
463 absorbance at 450 nm, measured spectrophotometrically, reflects the amount of cyclic di-
464 AMP-HRP tracer bound to the well and is inversely proportional to the concentration of free c-
465 di-AMP present during incubation.

466 **Plaque Assay-** A recently developed protocol was followed[44]. Briefly, *H. volcanii* strains were
467 grown overnight in Hv-ECa medium and normalized to an optical density of 595 nm (OD595).
468 Next, 400 µl of cultures with 0.5 M CaCl2 was added to 3-4 ml of 0.2% top-agar (preheated
469 and cooled to 60°C) in Hv-YPC, and the mixture was spread onto rich agar plates with 18%
470 SW. The plates were incubated at room temperature for 15 to 20 minutes. A ten-fold serial
471 dilution of HFPV-1 was prepared in Hv-ECa, and 3 µl of each dilution was spotted onto the
472 agar. After 2 days of incubation at 30°C, plaques formed. The plates were then left on the
473 bench at around 25°C for 2-3 days, during which time the plaques continued to grow and
474 become more distinct. Images were captured to document the growth and appearance of the
475 plaques.

476 **Long-term growth experiments-** Individual colonies were selected from each strain (the *H.*
477 *volcanii* strain containing H-TIR-SAVED and a control strain infected with the virus) and grown

478 in liquid Hv-ECa medium supplemented with thymidine and tryptophan until reaching late
479 logarithmic or stationary growth phase. The cultures were then subcultured into fresh medium,
480 and this process was repeated for approximately 3 passages. After the third passage, 100 µl
481 from each culture was serially diluted in fresh Hv-Ca medium and spread onto Hv-Ca plates
482 containing thymidine and tryptophan. From the resulting growth, 25-30 colonies from each
483 sample were analysed by PCR to assess HFPV-1 viral presence.

484 **Quantitative real-time PCR (Q-PCR)-** We determined the genome copy numbers of *H.*
485 *volcanii* and HFPV-1 using a CFX Connect Real-Time PCR system. Cultures were grown in
486 triplicate for 72 hours, after which we collected 1 ml samples and centrifuged them at 11,000
487 × g for 10 minutes at room temperature. To measure viral DNA secretion, we extracted DNA
488 from 200 µl of the resulting supernatant using a Quick-DNA Viral Kit. We then performed
489 quantitative PCR with q-PCRBIO SyGreen Blue mastermix Hi-ROX, using primers targeting
490 both an internal viral protein and the DNA polymerase II small subunit (*polB*), which served as
491 a housekeeping gene. The viral DNA measurements were normalized by comparing their cycle
492 threshold values to those of *polB*.

493 **Homology modelling using AlphaFold3**- To create a homology model of the H-TIR-SAVED,
494 we employed a multi-step process based on AlphaFold3 structure prediction. We first
495 extracted the amino acid sequence of the H-TIR-SAVED (accession number:
496 WP_115891642.1) from the NCBI database. The extracted sequence was submitted to the
497 AlphaFold3 server for predicted structure generation. After obtaining the model, we conducted
498 a Foldseek search for structural comparison against the PDB database. The resulting structure
499 was analysed based on TM-score and RMSD (Root Mean Square Deviation) values. Finally,
500 we used the UCSF Chimera software to visualize the alignments and generate the figures.

501 **Author contributions**

502 U.G. and D.K.C. conceived and designed the study. D.K.C. performed the experiments with
503 assistance from D.V. and H.S. D.K.C. also analyzed the data and prepared the figures. The
504 manuscript was written by D.K.C. and U.G. All authors read and approved the final draft.

505 **Acknowledgements**

506 The authors thank Prof. Sonja-Verena Albers for providing the strain with lower c-di-AMP
507 levels and for discussions about c-di-AMP signalling in archaea. We thank Dr. Mantu Kumar
508 for assistance with structure modeling and Alex Barbul for help with confocal microscopy. The
509 authors also thank Dr. Leah Reshef for helpful discussions.

510 **Funding**

This research was supported by the Israeli Science Foundation (grant 1599/24) and the European Research Council (grant AdG 787514).

Conflict of interest

The authors declare that they have no conflict of interest.

References

1. Culbertson, E. M. & Levin, T. C. Eukaryotic CD-NTase, STING, and viperin proteins evolved via domain shuffling, horizontal transfer, and ancient inheritance from prokaryotes. *PLOS Biol.* **21**, e3002436 (2023).
2. Millman, A., Melamed, S., Amitai, G. & Sorek, R. Diversity and classification of cyclic-oligonucleotide-based anti-phage signalling systems. *Nat. Microbiol.* **5**, 1608–1615 (2020).
3. Tesson, F. *et al.* Systematic and quantitative view of the antiviral arsenal of prokaryotes. *Nat. Commun.* **13**, 2561 (2022).
4. Cohen, D. *et al.* Cyclic GMP–AMP signalling protects bacteria against viral infection. *Nature* **574**, 691–695 (2019).
5. Lowey, B. *et al.* CBASS Immunity Uses CARF-Related Effectors to Sense 3'-5'- and 2'-5'-Linked Cyclic Oligonucleotide Signals and Protect Bacteria from Phage Infection. *Cell* **182**, 38-49.e17 (2020).
6. Duncan-Lowey, B., McNamara-Bordewick, N. K., Tal, N., Sorek, R. & Kranzusch, P. J. Effector-mediated membrane disruption controls cell death in CBASS antiphage defense. *Mol. Cell* **81**, 5039-5051.e5 (2021).
7. Hogrel, G. *et al.* Cyclic nucleotide-induced helical structure activates a TIR immune effector. *Nature* **608**, 808–812 (2022).
8. Rousset, F. *et al.* A conserved family of immune effectors cleaves cellular ATP upon viral infection. *Cell* **186**, 3619-3631.e13 (2023).
9. Ledvina, H. E. *et al.* An E1–E2 fusion protein primes antiviral immune signalling in bacteria. *Nature* **616**, 319–325 (2023).

537 10. Choudhary, D. K. *et al.* An archaeal CBASS system eliminates viruses without killing the host cells.
538 2024.09.12.612678 Preprint at https://doi.org/10.1101/2024.09.12.612678 (2024).
539 11. Govande, A. A., Duncan-Lowey, B., Eaglesham, J. B., Whiteley, A. T. & Kranzusch, P. J. Molecular
540 basis of CD-NTase nucleotide selection in CBASS anti-phage defense. *Cell Rep.* **35**, 109206 (2021).
541 12. Jacob, F. Evolution and Tinkering. *Science* **196**, 1161–1166 (1977).
542 13. Molecular and Genome Evolution - Hardcover - Dan Graur - Oxford University Press.
543 https://global.oup.com/ushe/product/molecular-and-genome-evolution-
544 9781605354699?cc=il&lang=en.
545 14. Wang, S. *et al.* The role of TIR domain-containing proteins in bacterial defense against phages.
546 *Nat. Commun.* **15**, 7384 (2024).
547 15. Wani, K. A. & Pukkila-Worley, R. Evolutionarily ancient functions of enzymatic TIR proteins in
548 innate immunity. *Trends Immunol.* **46**, 441–454 (2025).
549 16. Burroughs, A. M., Zhang, D., Schäffer, D. E., Iyer, L. M. & Aravind, L. Comparative genomic
550 analyses reveal a vast, novel network of nucleotide-centric systems in biological conflicts,
551 immunity and signaling. *Nucleic Acids Res.* **43**, 10633–10654 (2015).
552 17. Morehouse, B. R. *et al.* STING cyclic dinucleotide sensing originated in bacteria. *Nature* **586**,
553 429–433 (2020).
554 18. Ofir, G. *et al.* Antiviral activity of bacterial TIR domains via immune signalling molecules. *Nature*
555 **600**, 116–120 (2021).
556 19. Shi, Y. *et al.* Structural characterization of macro domain–containing Thoeris antiphage defense
557 systems. *Sci. Adv.* **10**, eadn3310 (2024).
558 20. Ka, D., Oh, H., Park, E., Kim, J.-H. & Bae, E. Structural and functional evidence of bacterial
559 antiphage protection by Thoeris defense system via NAD+ degradation. *Nat. Commun.* **11**, 2816
560 (2020).
561 21. Slavik, K. M. & Kranzusch, P. J. CBASS to cGAS-STING: The Origins and Mechanisms of Nucleotide
562 Second Messenger Immune Signaling. *Annu. Rev. Virol.* **10**, 423–453 (2023).

563 22. Binder, S. C. *et al.* The SAVED domain of the type III CRISPR protease CalpL is a ring nuclease.
564 *Nucleic Acids Res.* **52**, 10520–10532 (2024).
565 23. Steens, J. A., Salazar, C. R. P. & Staals, R. H. J. The diverse arsenal of type III CRISPR-Cas-
566 associated CARF and SAVED effectors. *Biochem. Soc. Trans.* **50**, 1353–1364 (2022).
567 24. Rouillon, C. *et al.* Antiviral signalling by a cyclic nucleotide activated CRISPR protease. *Nature*
568 **614**, 168–174 (2023).
569 25. Athukoralage, J. S. & White, M. F. Cyclic Nucleotide Signaling in Phage Defense and Counter-
570 Defense. *Annu. Rev. Virol.* **9**, 451–468 (2022).
571 26. Alarcón-Schumacher, T., Naor, A., Gophna, U. & Erdmann, S. Isolation of a virus causing a chronic
572 infection in the archaeal model organism Haloferax volcanii reveals antiviral activities of a
573 provirus. *Proc. Natl. Acad. Sci. U. S. A.* **119**, e2205037119 (2022).
574 27. Giani, M., Miralles-Robledillo, J. M., Peiró, G., Pire, C. & Martínez-Espinosa, R. M. Deciphering
575 Pathways for Carotenogenesis in Haloarchaea. *Mol. Basel Switz.* **25**, 1197 (2020).
576 28. Kellermann, M. Y., Yoshinaga, M. Y., Valentine, R. C., Wörmer, L. & Valentine, D. L. Important roles
577 for membrane lipids in haloarchaeal bioenergetics. *Biochim. Biophys. Acta BBA - Biomembr.*
578 **1858**, 2940–2956 (2016).
579 29. Vögeli, B. *et al.* Archaeal acetoacetyl-CoA thiolase/HMG-CoA synthase complex channels the
580 intermediate via a fused CoA-binding site. *Proc. Natl. Acad. Sci.* **115**, 3380–3385 (2018).
581 30. Abramson, J. *et al.* Accurate structure prediction of biomolecular interactions with AlphaFold 3.
582 *Nature* **630**, 493–500 (2024).
583 31. Abramson, J. *et al.* Accurate structure prediction of biomolecular interactions with AlphaFold 3.
584 *Nature* **630**, 493–500 (2024).
585 32. Ofir, G. *et al.* Antiviral activity of bacterial TIR domains via immune signalling molecules. *Nature*
586 **600**, 116–120 (2021).
587 33. Braun, F. *et al.* Cyclic nucleotides in archaea: Cyclic di-AMP in the archaeon Haloferax volcanii
588 and its putative role. *MicrobiologyOpen* **8**, e00829 (2019).

589 34. van der Does, C., Braun, F., Ren, H. & Albers, S.-V. Putative nucleotide-based second messengers
590 in archaea. *microLife* **4**, uqad027 (2023).
591 35. Galperin, M. Y. All DACs in a Row: Domain Architectures of Bacterial and Archaeal Diadenylate
592 Cyclases. *J. Bacteriol.* **205**, e00023-23 (2023).
593 36. DeWeirdt, P. C., Mahoney, E. M. & Laub, M. T. DefensePredictor: A Machine Learning Model to
594 Discover Novel Prokaryotic Immune Systems. 2025.01.08.631726 Preprint at
595 https://doi.org/10.1101/2025.01.08.631726 (2025).
596 37. Hobbs, S. J. *et al.* Phage anti-CBASS and anti-Pycsar nucleases subvert bacterial immunity. *Nature*
597 **605**, 522–526 (2022).
598 38. Cao, X. *et al.* Phage anti-CBASS protein simultaneously sequesters cyclic trinucleotides and
599 dinucleotides. *BioRxiv Prepr. Serv. Biol.* 2023.06.01.543220 (2023)
600 doi:10.1101/2023.06.01.543220.
601 39. Makarova, K. S. *et al.* Evolutionary and functional classification of the CARF domain superfamily,
602 key sensors in prokaryotic antivirus defense. *Nucleic Acids Res.* **48**, 8828–8847 (2020).
603 40. Whiteley, A. T. *et al.* c-di-AMP modulates Listeria monocytogenes central metabolism to regulate
604 growth, antibiotic resistance and osmoregulation. *Mol. Microbiol.* **104**, 212–233 (2017).
605 41. Oppenheimer-Shaanan, Y., Wexselblatt, E., Katzhendler, J., Yavin, E. & Ben-Yehuda, S. c-di-AMP
606 reports DNA integrity during sporulation in Bacillus subtilis. *EMBO Rep.* **12**, 594–601 (2011).
607 42. Zarrella, T. M. & Bai, G. The Many Roles of the Bacterial Second Messenger Cyclic di-AMP in
608 Adapting to Stress Cues. *J. Bacteriol.* **203**, e00348-20 (2020).
609 43. Govande, A. A., Duncan-Lowey, B., Eaglesham, J. B., Whiteley, A. T. & Kranzusch, P. J. Molecular
610 basis of CD-NTase nucleotide selection in CBASS anti-phage defense. *Cell Rep.* **35**, 109206 (2021).
611 44. Navok, S., Cohen, L., Ron, E. Z. & Gophna, U. Optimized Plaque Assay for Detecting Chronically
612 Infecting Viruses of Haloarchaea. 2024.11.12.619373 Preprint at
613 https://doi.org/10.1101/2024.11.12.619373 (2024).